# Optimization of illumination schemes in a head-mounted display integrated with eye tracking capabilities

Craig W. Pansing[a], Hong Hua*[a], Jannick P. Rolland[b]
[a]The University of Arizona, College of Optical Sciences, Tucson, AZ USA 85721
[b]The University of Central Florida, College of Optics and Photonics, Orlando, FL USA 32816

## ABSTRACT

Head-mounted display (HMD) technologies find a variety of applications in the field of 3D virtual and augmented environments, 3D scientific visualization, as well as wearable displays. While most of the current HMDs use head pose to approximate line of sight, we propose to investigate approaches and designs for integrating eye tracking capability into HMDs from a low-level system design perspective and to explore schemes for optimizing system performance. In this paper, we particularly propose to optimize the illumination scheme, which is a critical component in designing an eye tracking-HMD (ET-HMD) integrated system. An optimal design can improve not only eye tracking accuracy, but also robustness. Using LightTools®, we present the simulation of a complete eye illumination and imaging system using an eye model along with multiple near infrared LED (IRLED) illuminators and imaging optics, showing the irradiance variation of the different eye structures. The simulation of dark pupil effects along with multiple 1st-order Purkinje images will be presented. A parametric analysis is performed to investigate the relationships between the IRLED configurations and the irradiance distribution at the eye, and a set of optimal configuration parameters is recommended. The analysis will be further refined by actual eye image acquisition and processing.

**Keywords:** Illumination; Eye tracking; Head-mounted display; Wearable displays; Displays

## 1. INTRODUCTION

Since the first developments of head mounted displays (HMDs) originated from Ivan Sutherland in the 1960s [1], HMDs have been explored for applications that enhance human-computer interfaces through three-dimensional (3D) computer-generated or synthetic environments. These applications include 3D scientific visualization, interactive control, education and training, telemanipulation, tele-presence, wearable computers, and entertainment systems. The broad use of HMDs has spawned many different forms of wearable displays, such as immersive HMDs, where the user is presented a view that is under full control of a computer at the expense of the physical view [2]; optical see-through HMDs (ST-HMDs) that superimpose virtual objects optically to enhance the physical scene [3]; video see-through HMDs that electronically combine virtual objects with a real scene captured through video cameras [4]; virtual retina displays that rapidly scan low-power laser beam directly across the retina to form a 2D image [5]; and head-mounted projective displays that utilize the combination of projection optics and retro-reflective material to optically combine virtual objects with the physical scene [6,7].

The technology has been hindered by trade-offs in capability and limitations of resolution and field of view (FOV), distortion for wide FOV designs, inaccurate eye point representation, decoupled cues of accommodation and convergence, the occlusion contradiction between virtual and real objects, precise registration, weight and volume, and often brightness conflicts with a bright background illumination [8]. While many of these limitations have been explored at length, the consideration of eye movement has commonly remained a completely separate topic, and minimal effort has been made to merge HMD and eye tracking technologies to explore the benefits and optimization of an integrated system.

Partly, this problem of combining wearable displays and eye tracking may be due to the slow evolution of eye tracking. Various forms of eye tracking have been researched since the sixteenth century, and numerous techniques are available

*Email: hhua@optics.arizona.edu; Phone 1 520 626 8703; Web: http://3dvis.optics.arizona.edu

to track the eye.  However, the need for efficient eye tracking has been highlighted by the wide number of research efforts in the fields of cognition, human-computer interaction (HCI), psychology, human performance and marketing.

In these applications, the techniques used to determine gaze information generally fall into three categories: electro-oculography (EOG), scleral search coil, and reflection based approaches [9].  Each of these categories has advantages and drawbacks to the application of HMDs, which will be discussed.

The EOG method utilizes the electrical potential generated by the muscles in the eye-socket when the eye moves.  If electrodes are attached around the eye to measure this potential, eye movements can be detected. [10,11]  This approach is very simple, but has poor accuracy and is very invasive, which limits its effectiveness in practical eye tracking and HMD integration.  In the scleral search coil approach, an induction coil is implanted into the subject's eye surgically or the subject must wear custom contacts in order to detect eye movements [12].  While the method is very accurate, which is beneficial for the system implementation, it can be extremely invasive and is seldom used for human subjects. Reflection based approaches are a more recent development of eye tracking.  These reflection methods utilize near infrared (NIR) light to illuminate the eye and some type of imaging system to capture images.  Image processing is done on these images to identify various features of the eye for a mapping process that must be performed on each user to determine the gaze direction of the eye [13].  The different types of reflection based approaches are characterized by the features detected and the configuration of the light source (typically IRLEDs) [14,15].  Of the available eye tracking techniques, reflection approaches have the advantage of being non-invasive and acceptably accurate, so are therefore applicable to practical HMD integration.

Previous attempts at implementing the HMD and eye tracking technologies have generally been high-level by simply combining established HMDs and eye trackers.  For example, ISCAN, a commercial eye tracking company, integrated their eye tracker product with VR4 and V8 HMDs from Virtual Research.  The Virtual Reality Eye Tracking Lab of the Computer Science Department at Clemson University has been using a V8-integration by ISCAN to conduct research related to gaze-contingent virtual environments [16].  The use of existing HMDs and eye trackers allows for exploration into the benefits of a combined system, but it is impossible to take advantage of benefits that would be gained from implementing the two systems from a low-level approach to achieve complete integration.

Beach et al. [17] and Vaissie et al. [18] have made some efforts to achieve complete integration with low-level optimization. Iwamoto et al. [19-22] is developing an integrated system using scan mirrors to present a high-resolution, low FOV image over a low-resolution, high FOV background dependent on the gaze direction of the user to relax the resolution and FOV tradeoff.  Rolland et al. [23] considered a high resolution inset HMD with eye tracking using lenslets for high resolution image movement. While these systems attempt eye tracking and HMD integration, none of the research has considered the advantage of using the rigid nature of the HMD to position LEDs in an optimized pattern to illuminate the eye and thus obtain well controlled eye images for efficient eye tracking.

The subject of this paper is to present an optimized illumination scheme to obtain "well-illuminated" eye images that result in accurate and robust detection of eye features.  To accomplish this task, a non-sequential ray trace program (LightTools® [24]) was used to construct a model containing illuminators, a simple eye structure, and an imaging system. This model was used to test different LED parameters specific to typical HMD designs to determine which combinations provide a well illuminated eye.  The results of this study are presented, along with a recommendation for an illumination pattern suitable for integrated systems. The organization of this paper is as follows.  In section 2, the overall architecture of the HMD and eye tracker implementation is discussed.  Section 3 describes the simulation setup used to find the optimized illumination pattern.  Section 4 presents the different LED parameters tested and simulation results.  Section 5 describes the process used to investigate the simulation results.

## 2.  OVERALL ARCHITECTURE FOR THE EYE TRACKING - HMD INTEGRATION

In an eye tracking-HMD (ET-HMD) integrated system, there are two optical paths:  one path containing the HMD optics that presents the user with magnified images displayed on miniature displays; the other containing the eye tracking optics that illuminates the user's eye and captures eye images for tracking processing.  While some efforts have been made to develop integrated systems, in the systems that adopt stand-alone HMDs and eye trackers for

integration, the two optical paths are mostly separated from each other and the integration is only functional. A systematic approach is required to optimize the overall architecture and to achieve a compact, comfortable, easy-to-use, and reliable system.

An example of a systematic integration design is shown in Figure 1, in which the HMD and eye tracker paths are combined to share optical elements, which allows the reduction of weight and volume for an integrated ET-HMD system [14]. The ray-tracing for the HMD path is shown in the Figure 1(a), while the ray-tracing for eye imaging is shown in Figure 1(b). The display path in the ET-HMD is essentially the same as a classical HMD path. The light from a miniature display travels through a hot mirror to the eyepiece optics, which forms a magnified image for the user. In the eye tracking path, one or multiple IRLEDs are mounted around the eyepiece or at locations near the eye to provide adequate illumination. The off-axis IR illumination creates a dark-pupil effect and forms virtual images of the LEDs, classified as 1st-order Purkinje images or glints. The dark pupil, 1st-order Purkinje images, and other eye structures are then imaged by the same eyepiece as the HMD paths, and further reflected off the hot mirror and captured by an infrared CCD for gaze-direction tracking.
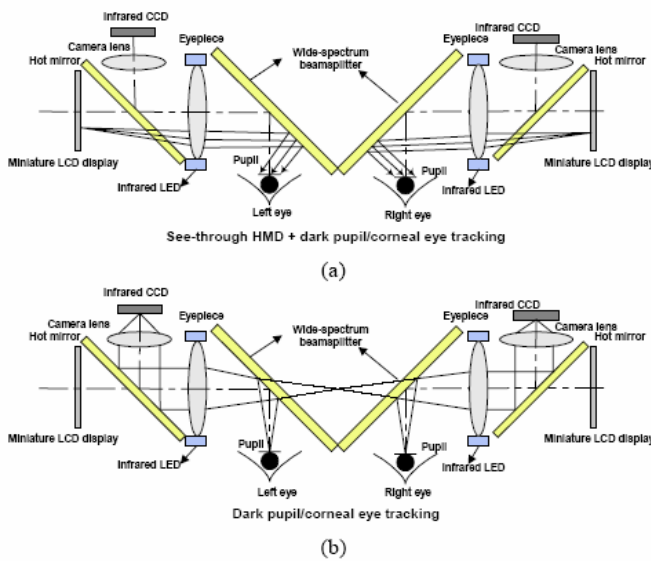


Figure 1: Overall architecture concept for ET-HMD integration. (a) Optical path for the HMD; (b) Optical path for the pupil/corneal reflection eye tracker

Understanding the processing of the eye image for gaze-direction tracking is vital to determining the "optimized" illumination pattern that should be incident upon the eye. Figure 2 shows the segmentation of a pupil from an IR-illuminated eye image. Present in the image are two important features that will be used in the eye tracking: the dark pupil and the 1st-order Purkinje images of the IRLEDs formed by the reflection of the anterior cornea surface. Most light incident upon the eye is scattered off the features surrounding the eye and imaged by the imaging optics, while the pupil becomes a sink for the off-axis light traveling through the pupil. Therefore, the pupil usually appears darker than the other eye features and a sharp barrier between the dark pupil and the iris is formed. Using this pupil-iris boundary, the pupil center can be identified and mapped to a gaze direction of the eye. A typical eye tracking algorithm will start by setting adequate thresholds to segment out the pupil from the rest of the eye features. This step is followed by a series of erosions and dilations using a predefined kernel to close any potential holes and obtain a sharp pupil edge. Using an edge detection algorithm, an ellipse can be fit around the pupil to establish a pupil center [25]. The next important features in the eye image are the glints through corneal reflections. A similar thresholding algorithm can be used to segment out the glints and calculate their locations in the eye images. A mapping of the center of the pupil and the center of the glints can then be used to calculate the point-of-regard of the eye [14]. Utilizing both the pupil and glint features provides for robust tracking that is tolerant to head movement to some extent.

Real-time and reliable detection of the pupil boundary and glints is key to an accurate eye tracking system. Simple segmentation methods are preferred for both pupil and glint detection to facilitate real-time implementation. The thresholding approach is perhaps the simplest and most efficient segmentation algorithm, as grey levels of the pupil and glints are distinguished reliably from the histogram of an eye image without the need for a complicated algorithm. Furthermore, sufficient contrast between the features of interest and other eye structures and the sharpness of the feature boundary are crucial to the robustness of eye tracking. For instance, in a well-illuminated dark-pupil IR image, the pupil will be the darkest feature while the glints will be the brightest ones and as a result, appropriate thresholds are set to directly segment out these features.

Figure 2:    The steps involved in finding the center of the pupil (a) aquire the native eye image (b) threshold the image (c) perform a closing operation to remove holes (d) fit an ellipse to estimate the center and shape of the pupil

Appropriate illumination of the eye can aid the tracking algorithms to make thresholding, and therefore segmentation, of the pupil and glints easier.   However, obtaining high-contrast images is challenged by various illumination factors. For illumination that is not optimized, segmenting the pupil may be difficult, while segmenting the glints may become difficult when some part of the eye is over-illuminated, or specular reflections exist to disguise the glints.   Another challenge is that the quality of eye illumination often varies with different users of the potential device due to different feature reflectances.   The purpose of this study is to investigate the various parameters that potentially affect the quality of eye illumination, and identify illumination schemes that lead to high-contrast eye images for post-processing.

## 3.  SIMULATION SETUP

In order to determine an optimized illumination configuration, the optical model of an arbitrary pupil-glint based eye tracking system was developed using LightTools®. This model consisted of a set of IRLEDs, an eye model with basic optical surfaces and non-optical structures, imaging optics, and an image sensor. This section will detail the procedures for modeling each of the major components in the system and present simulated results.

### 3.1.  LED modeling

To create illumination for an eye tracking system, there are many available LEDs that may be selected.   One of the major factors to be considered for LED selection is the nominal angular range in which the light emitted by an LED is distributed.   This range, defined as the spread angle of an LED, is presented by the relative radiant intensity curve as a function of angle.   In an eye tracking system, the spread angle is required to sufficiently illuminate approximately a 40 x 30mm eye area, which we estimated from measurements on a pool of human subjects, over a given distance.   In the case of an ET-HMD, the illumination distance is usually constrained by the eye relief of HMD optics, which is typically 20mm to 70mm for most immersive and see-through HMDs.   Therefore, a wide angle LED is desirable.   If a single LED is utilized, a spread angle of up to 90 degrees is desired for a distance of 20mm, or 40 degrees for a distance of 70mm.   However, utilizing multiple LEDs can significantly relax the requirements for LED spread angles.   Four LEDs were used in our simulation setup for the sake of symmetry.   For the four LEDs, a 45 degree spread angle would roughly satisfy the illumination requirement over a minimal distance of 25mm. Another factor to consider is the wavelength spectrum. Near-infrared LEDs were selected to minimize user distraction by the LEDs and to ensure that a regular black-white CCD detector with reasonable infrared response could be used, rather than a more expensive infrared sensor.

To meet these requirements for spread angle and wavelength, we selected four IRLEDs, model BIR-BO07J4Q-1 by American Bright, which have a spread angle of 45 degrees and a wavelength of 850nm. In LightTools®, the geometry of these modeled LEDs were spheres of diameter 5mm to match the size of the physical LEDs. The intensity distribution of the LEDs was modeled using an apodization file generated from the specifications provided by the manufacturer. The accuracy of the simulated LEDs was verified to within ±18 degrees to closely match the angular distribution measured from the physical LEDs as shown in Figure 3.
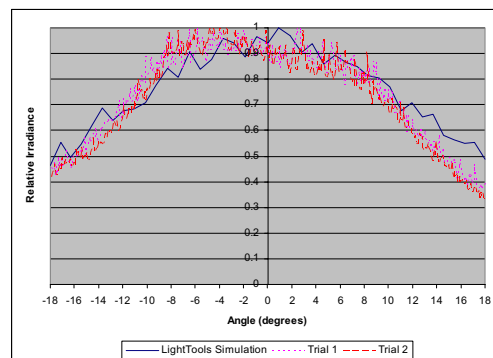


Figure 3:    LED model verification

## 3.2. Eye structure modeling

To develop a complete imaging model, it is necessary to model the optical surfaces and the basic non-optical structures of a human eye. Accurate representation of the optical surfaces of the human visual system allows the appropriate imaging of the glints, pupil, and iris features; and accurate modeling of selected non-optical structures allows the simulation of other related eye features such as the sclera, eyelid, and surrounding skin.

While several other models exist [26], the Arizona Eye Model [27] as shown in Table 1 was adopted as the optical prescription of a human eye. A snapshot of the eye optics model in LightTools® is shown in Figure 4(a). All refractive elements except the anterior cornea were assigned 100% transmittance. The anterior cornea has been modeled with approximately 97.6% transmittance and 2.4% reflectance to allow for glint formation. The reflectance was approximated by finding the Fresnel reflectance at normal incidence. [28]

Modeling the non-optical structures and their associated properties is somewhat empirical and achieving good accuracy has proved to be a challenge. An 11mm circular structure has been modeled at the iris, which appropriately encloses the aperture of the anterior lens. A large 7mm pupil has been modeled to overlap with the glints for convenience. Surrounding the eye optics, spherical structures and cylinders of various radii were heuristically modeled to simulate the sclera, eyelid, eyebrow, cheek and nose features. These non-optical structures were framed within a 40mm x 30mm eye area, estimated from a pool of human subjects, which takes into account potential slippage of the ET-HMD. A snapshot of the modeled eye structure is shown in Figure 4(b).

Characterizing the reflectance of the non-optical eye structures and the surrounding skin accurately has proved to be difficult due to the lack of measured data available in the existing literature. Perhaps the closest research was reported by Marshner et al. [29] at Cornell University, in which a photographic approach was used to measure the bidirectional reflectance distribution function (BRDF) of human skin at visible wavelengths. While both diffuse and specular reflections might be present, for simplicity and speed of simulation computation, we treated each of the surfaces as Lambertian, and thus potential specular reflections caused by tears and sclera were not modeled. The feature reflectances were heuristically estimated from an eye image taken under a quite uniform illumination upon the eye. The reflectance parameters emphasized in this paper are given in Table 2 and match the Caucasian skin and a blue iris.

|  | Radius (mm) | Conic | Thickness (mm) | nd | nf | nc |
|---|---|---|---|---|---|---|
| Anterior Cornea | 7.8 | -0.25 | 0.55 | 1.3771 | 1.3807 | 1.37405 |
| Posterior Cornea | 6.5 | -0.25 | 3.05 | 1.3374 | 1.3422 | 1.3354 |
| Anterior Lens | 11.03 | -4.3 | 4 | 1.42 | 1.42625 | 1.4175 |
| Posterior Lens | -5.72 | -1.17 | 16.6423 | 1.336 | 1.3407 | 1.3341 |
| Retina | -13.4 |  |  |  |  |  |

Table 1: Arizona Eye Model Prescription
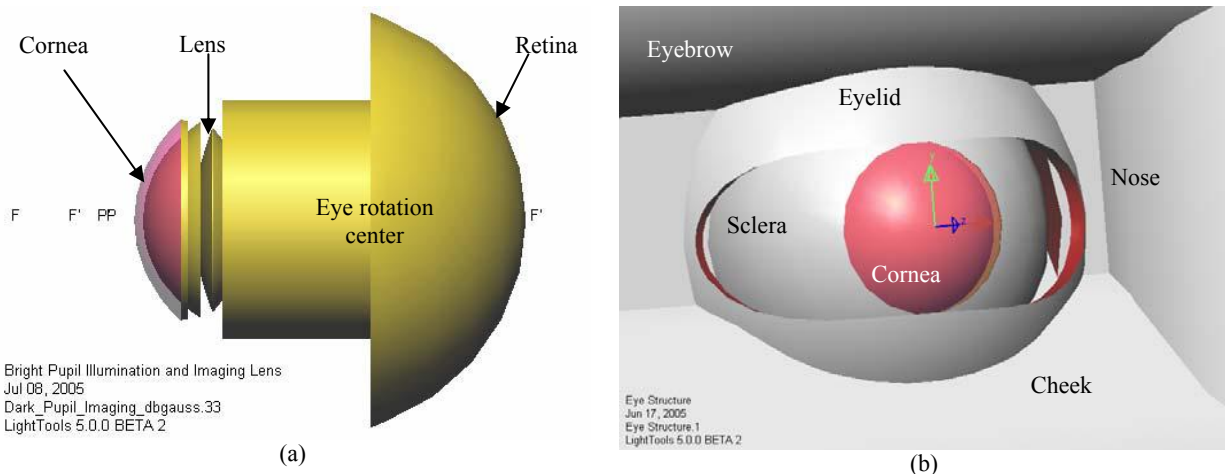


(a)



(b)

Figure 4: LightTools® models of the (a) eye optics and (b) complete eye model

### 3.3. Imaging optics modeling

An imaging system is required to simulate the image of the illuminated eye on the image plane. While we initially tried to design an optical system that accounted for the sharing of optical elements between the HMD and eye tracker paths, as shown in Figure 1, we discovered that such a design had a large F-number. Consequently, such a system is not effective for ray tracing in

| Feature | Reflectance | Surface Type |
|---------|-------------|--------------|
| Cornea | 2.4% | Optical |
| Iris | 5% | Lambertian |
| Sclera | 9% | Lambertian |
| Skin | 12% | Lambertian |

Table 2:   Eye reflectance values

LightTools®, and a large number of rays have to be traced to create a reasonable irradiance on the image plane. Indeed, the imaging system in the simulation setup is not required to resemble the optical design in an actual ET-HMD design as the main concern hereby is the illumination quality, rather than the complexity of an end system or the imaging quality. Therefore, maximizing the effective aperture size to collect more rays becomes a critical consideration for computation speed.

A Double Gauss lens obtained from a U.S. Patent [30], with an effective focal length of 125.7mm and an F-number of 2.51, was modified and optimized to meet wavelength and finite imaging requirements in the simulation setup. The wavelength modification to the original design was to use an 850nm wavelength, rather than the visible spectrum for which it was originally designed. The finite imaging modification was to set the system to image the conjugate of the eye plane, which is located at a finite distance rather than infinity as the original lens was designed. Optimization was made to achieve reasonable imaging performance. The layout of the modified system is shown in the Figure 5 and its prescription is listed in Table 3.

### 3.4. The simulated system and results

The LEDs, eye structure, and imaging optics described above have been assembled into a system and a snapshot of the model is shown in Figure 6(a). The rays from the IRLEDs illuminate the eye area and are transmitted through or reflected off the eye optics and scattered by other non-optical eye structures. The reflected and scattered rays are then focused by the imaging optics onto its conjugate image plane.

The magnification of the desired eye area dictated the image plane size. Instead of actually modeling a physical sensor, LightTools® allows the image plane to be divided into a large number of bins, each of which collects rays through the imaging optics. The number of bins determines the resolution of the raster image rendered by the ray tracing engine.
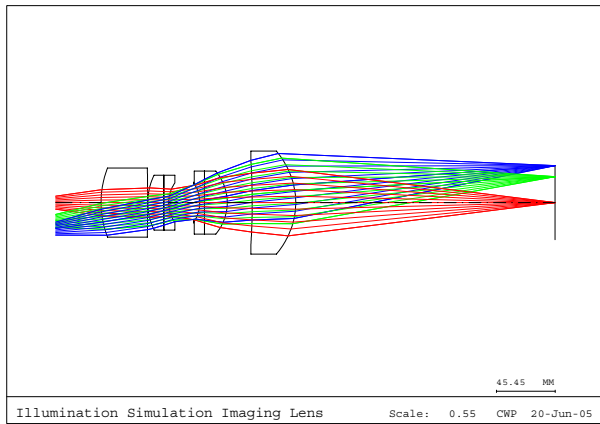


Figure 5:   Layout of the imaging lens

| Surface | Radius | Conic | Thickness | Glass |
|---------|--------|-------|-----------|-------|
| Object | Infinity | | 70.00 | |
| 1 | 74.94 | 0.48 | 36.00 | BSM24 |
| 2 | -1279.02 | -2709 | 0.10 | |
| 3 | 47.96 | -0.2 | 12.42 | SK1 |
| 4 | Infinity | | 3.78 | F15 |
| 5 | 26.64 | -0.13 | 19.24 | |
| Stop | Infinity | | 4.69 | |
| 7 | -28.61 | 0.48 | 3.78 | F15 |
| 8 | Infinity | | 17.59 | SK16 |
| 9 | -37.62 | -0.08 | 19.29 | |
| 10 | -549.41 | 58.87 | 33.67 | SK16 |
| 11 | -57.85 | -0.36 | 200.46 | |
| Image | | | | |

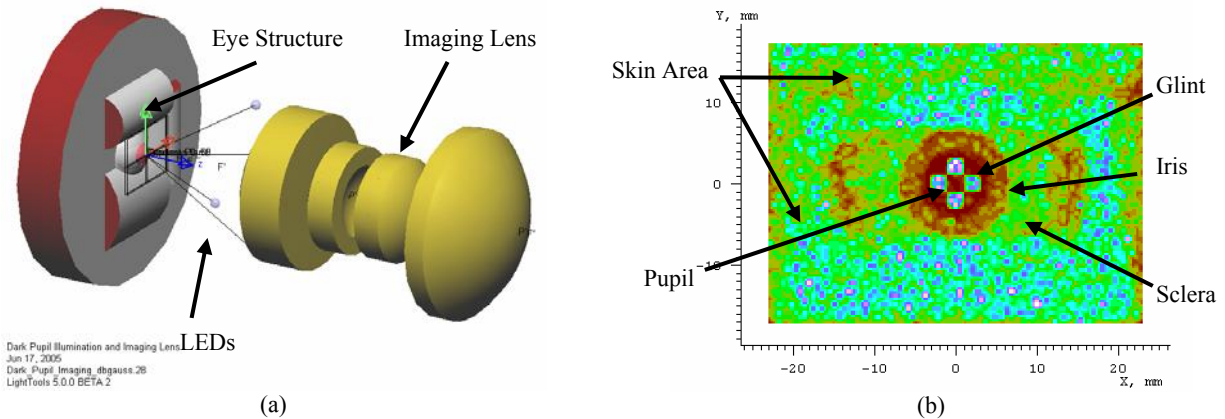Table 3:   Prescription of the imaging lens

Figure 6: (a) Complete simulated model with eye structure, LEDs and imaging lens (the image plane is not shown). (b) Sample image plane irradiance plot.

Ideally, the number of simulated bins should match the number of detector pixels, but the computational cost will be significant due to the finite nature of the simulation. To keep a reasonable computation speed, we divided the image plane into 87 x 65 bins (the size of the image is 46mm x 34.3mm, close to 1:1 magnification). By tracing about 1-1.5 million rays, this resolvability allowed a decent simulation of eye images that could be analyzed for quality assessment. A sample eye image, tracing 1.5 million rays, is shown in Figure 6(b), which is simulated by placing four IRLEDs symmetrically at an angle of 20 degrees, height of 30mm, and axial distance of 70mm. A simulation in this configuration takes approximately 20 minutes to run on a Pentium 4, 3.2GHz computer with 1GB RAM. Increasing the resolvability, at the cost of computation speed, is expected to improve the quality of the simulated image and thus improve the accuracy of optimization discussed in Section 4.

## 4. ILLUMINATION OPTIMIZATION

To identify optimal illumination configurations and to understand how the LED settings affect the quality of eye illumination, an optimization scheme, illustrated in Figure 7, has been developed. The scheme is divided into two steps: (1) generation of a user-defined illumination pattern; (2) evaluation of the input illumination pattern. The two steps are iterated to search through a database of irradiance distribution patterns until the illumination quality meets a set of given requirements. The pattern that yields the highest quality rating is considered the optimal illumination. This optimization process will be detailed in the following sub-sections.

### 4.1. Illumination generator

The purpose of the generator is to determine the position and angle settings of multiple LEDs, by using the LightTools® ray tracer and optimizer, which yield an illumination pattern that best matches a user-defined irradiance distribution function. These resultant LED settings (i.e. the specified illumination pattern) are then fed into the illumination-imaging simulation system.

### 4.1.1. Parametric definition

It is apparent that the selection and placement of LEDs play the most critical role in affecting the quality of eye illumination. In this paper, an emphasis is given to the geometric placements of the 45-degree American Bright LEDs selected in Section 3, without considering the effects of different spread angles or radiance distributions. The varied parameters that specify the placement of an LED are shown in Figure 8. Considering that multiple LEDs are to be mounted symmetrically surrounding the optical axis in the horizontal and vertical directions, only two distances are used to vary the location of an LED: the height, Y, of the LEDs from the optical axis and the distance, Z, from the cornea vertex of the eye along the optical axis. This height variation (Y) is expected to shift the illumination distribution incident on the eye, while the distance Z is expected to control the size of the illumination area. In an ET-HMD system, the range of the LED height is often constrained by the aperture of the optics in an end-system design and the interpupillary distance of a user. A range from 20mm to 40mm has been considered. Furthermore, the range of the

LED distance is often constrained by the eye relief required in an HMD system. Ranges from 20mm, the typical eye relief for immersive HMDs, to 70mm, for optical see-through HMDs eye relief, have been considered.
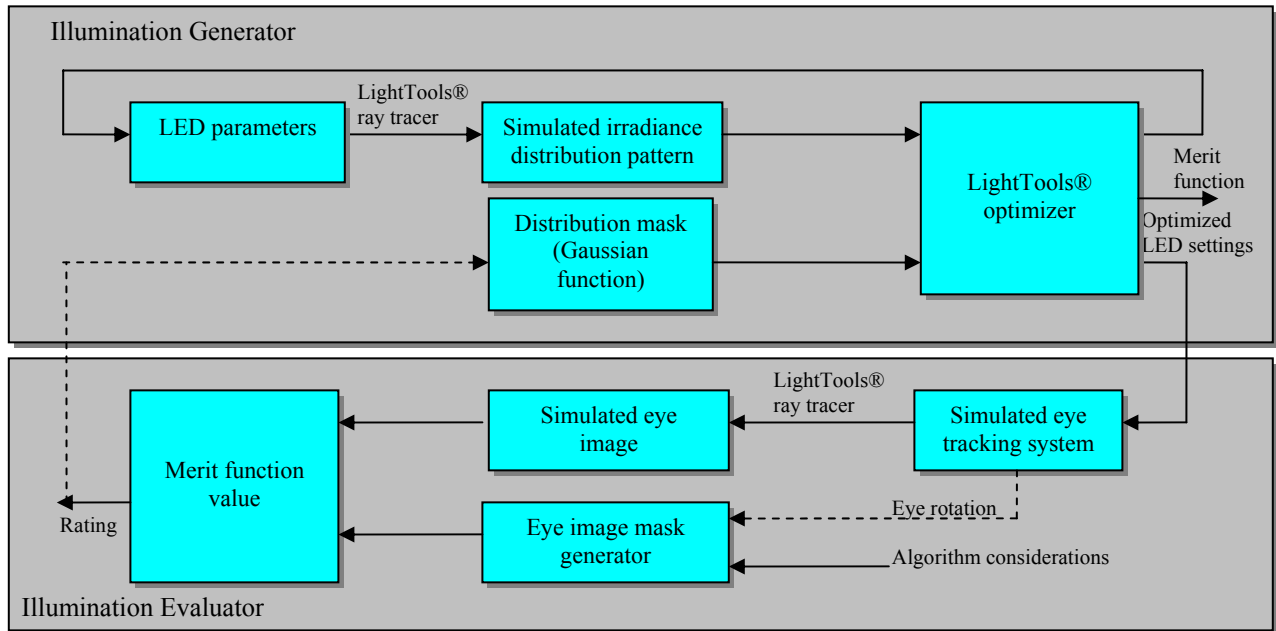


Figure 7:    Optimization scheme consisting of the illumination generator and illumination evaluator

The placement of an LED is further characterized by its orientation. The pitch of an LED relative to the optical axis is defined as $\theta$ and it is expected to affect the peak location of the illumination contribution by the given LED. The pitch is varied across the range of 0 degrees, where the LED pointing is parallel to the optical axis, to 30 degrees where the LED is tipped toward the optical axis. It is assumed that the irradiance distribution pattern of the LEDs is symmetric about their axis; neither the yaw nor the roll about the LED axes needs to be considered to maintain symmetrical placement. The final constraint for the LED placements is, as in any LED configuration, the requirement that multiple LEDs will be translated or pitched symmetrically relative to the optical axis.
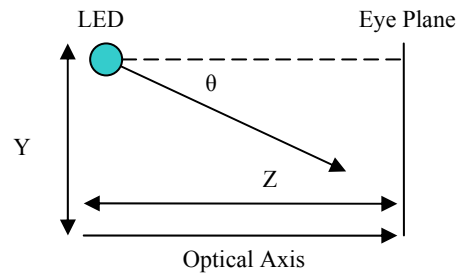


Figure 8:    LED positioning parameters

### 4.1.2.   Generation of user-defined illumination pattern

As indicated in Section 3, tracing millions of rays takes a considerable amount of computation time to create a simulated eye image. Searching through the LED parameter space to determine a "better" LED configuration will take a large number of simulation loops and thus a tremendous amount of time.

To speed up the computation and simplify the optimization process, an incident eye plane is introduced to the simulated illumination-imaging system as a secondary receiver. The plane is located at the cornea vertex of the eye and parallel to the XY reference plane, and its dimension is determined by the eye area of interest. Naturally, rays emitted from the LEDs create an irradiance distribution pattern, which serves as the input illumination to the eye optics, on the incident eye plane. Regardless of LED placements, which are often dependent upon a particular system design, an illumination scheme can be characterized by the distribution pattern on the eye plane.   Providing a user-defined distribution pattern, the LightTools® optimizer can be utilized to determine the optimal LED configurations that output an illumination

pattern on the eye plane that best match the function. The problem of optimizing eye illumination thus becomes a process of searching for an optimal distribution pattern on the eye plane. While this seems a simple task, tracing rays directly from LEDs to a plane receiver is much simpler and more computationally efficient than tracing through the imaging system to form an eye image.

A user-defined illumination pattern may be specified by a numerical function of an arbitrary irradiance distribution curve. While other functions might be utilized, we have chosen a 2D normal distribution with a falloff ratio of δ at the diagonal corner of the eye plane to characterize an illumination function. This function is treated as a reference or a mask on the eye plane. Due to the discretized nature of the ray tracer, the eye plane receiver has been divided into 21 x 15 bins, in a way similar to how the image plane was segmented, and the mask function has also been digitized as a 2D table by the same number of steps as in the eye plane's division.

To generate an illumination pattern with a given distribution, a parametric optimization is performed over the range of the LED parameters defined above to determine the optimal LED placements that yield a pattern having the best match with the reference function. Initially, the parameters of LED placements are digitized by steps over their corresponding range. For instance, the height Y is in 5 steps by an increment of 5 mm, the distance Z is in 11 steps by increments of 5mm and the angle θ is in 7 steps by increments of 5 degrees for a total of 385 steps.   The digitized parameters have been compiled into a spread sheet and an Excel® macro was created to interact with the LightTools optimizer.   A set of LED parameters is fed into the ray tracer of the simple LED-eye plane system and a simulated irradiance pattern is generated. This pattern is then compared against the mask function and a merit function value is generated by the LightTools® optimizer. Through the Excel® macro, the optimizer automatically loops through the LED parameter space to determine the distance and angle combination that yields a pattern having the closest match with the reference function.

## 4.2. Illumination evaluator

The purpose of the illumination evaluator is to evaluate the quality of an input illumination pattern by comparing the simulated eye image with an ideal eye image generated by a mask generator. Once a user-defined illumination pattern is generated, the resultant LED settings are then fed into the illumination-imaging simulation system and the ray tracer outputs a simulated eye image as shown in Figure 6(b). However, to find a "good" eye image, we require a sufficient rating mechanism. Since the complex structure of a simulated eye image is not readily qualified by direct evaluation means, we have developed an experimental evaluator based upon some basic heuristics of eye image analysis. Our evaluator compares a simulated eye image against a reference image generated by a mask generator as discussed below.

### 4.2.1.  Ideal eye image and mask generator

Ideal image quality heuristics are determined by considering the algorithm methods used to process the image and consequently find the gaze direction.  Typically, these algorithms use histogram data from the eye images as the important eye features can be segmented by relative brightness.   By maximizing feature brightness separation, an ideal image may be constructed that emphasizes important eye image features such as the pupil boundary and glints in particular.   Image considerations reflect the desired relative brightness of each feature for efficient tracking, as well as feature dimensions on the eye image.   A spreadsheet containing the ideal image values is then imported into the simulation model as a mask for comparison against a simulated eye image as a function of input parameters, a process similar to that described in section 4.1.2.

For the example of pupil tracking, which is part of the tracking method in the proposed ET-HMD, the pupil boundary is an important feature to consider for pupil center calculations.  The histogram data of an eye image with large brightness separation of the pupil compared to the remaining eye features yields a clear valley between feature values, that when maximized, computations to segment the pupil area become more efficient.   As shown in Figure 9(a), the ideal image mask we used for a dark pupil system particularly emphasizes the brightness uniformity of the pupil and surrounding skin areas as well as the high contrast of the pupil-iris boundary.   It is likely then that the incident illumination plane will be brighter in the center of the distribution pattern to compensate for the lower reflectance of the inner features.   Similar masks may be generated to emphasize the importance of other eye features, and a series of masks may be used to consider eye rotation into the optimization.
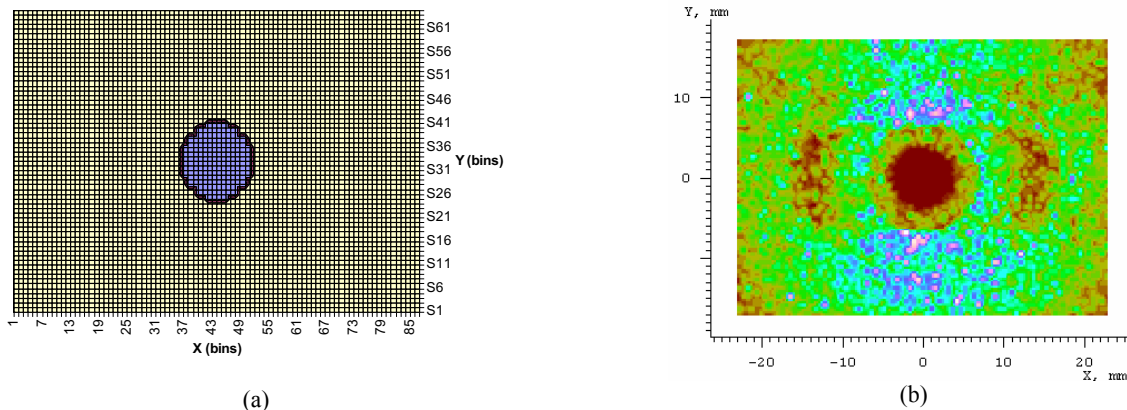
Figure 9:   (a) A 2D mask to optimize pupil tracking and (b) a simulation result using the pupil mask

## 4.2.2.  Quality evaluator

Eye images created by a particular illumination pattern are given a rating based on a merit function generated by the LightTools® optimizer for comparison among tested input distribution functions.   A minimized merit function value indicates a closer match to the ideal eye image.   The unique reference mask for the proposed system considered both the pupil and glint features, which suggested a need for a maximized difference between the pupil and skin, along with the glints and skin.   The importance of skin uniformity is apparent because any extreme non-uniformity may lead to erroneous pupil or glint segmentation.   While the 1st-order Purkinje images in an eye image mask are much greater in brightness compared to the skin area, this relationship excludes the loss of signal due to saturation of the glint pixels on a physical CCD camera.   Therefore the actual proportions of the pupil, skin, and glint features are unknown.   The LightTools® model described in this paper does not have the capability to simulate detector saturation, thus the proportions of an image mask containing both glint and pupil features are also unknown.   Since the glints are assumed to saturate the image, and the aperture size controls the pupil and skin proportions, we simulated the system by considering only the pupil boundary and the skin area uniformity.   The glints have been removed from the model by changing the cornea reflectance in LightTools® to 0% and the absorption to 2.4% so that no glints are formed at the eye image plane.   The mask in Figure 9(a) fulfills the boundary and uniformity conditions, and Figure 9(b) shows a simulated eye image using the pupil mask with the glints turned off.

## 4.3.  Iteration and results

The illumination generation steps described in section 4.1 are iterated to search through a database of irradiance distribution functions, which define various illumination patterns on the eye plane, until the illumination quality meets a set of given requirements. The parameters that yield the lowest merit function value are considered as the optimal illumination configuration for the particular pattern. In the experiment, a set of normal distributions, with the falloff value δ at the corners of the incident plane ranging from 0 (no falloff), corresponding to a uniform distribution, to 0.8 (80% falloff), being a steep distribution, have been examined using an increment of 0.1 (10% falloff). The evaluation outlined in 4.2 shows a merit value for δ equal 0 is 380.5, and the rating for δ equal 0.8 is 459.1.   Among the nine input functions being examined, δ = 0.3 and δ = 0.5 yield similar minimum merit function values of 341.8 and 342.3, respectively, for the simulated eye images.   The simulated irradiance distribution pattern on the eye plane for the δ = 0.3 is shown in Figure 10(a) and the simulated eye image is shown in Figure 10(b). Correspondingly, the LEDs modeled in the system have been placed at a height of 40mm from the optical axis, 70mm from the eye, and at a pitch angle of 20 degrees.   Considering the increment of δ, if a normal distribution function is the requirement, the δ = 0.3±0.1 and the δ = 0.5±0.1 solutions yield similar results, thus a δ = 0.4±0.2 is recommended as a "good" illumination pattern on the eye plane. Indeed, for a generally-designed imaging system, the imaging optics and the actual photometric response curve of the CCD sensor are anticipated to have effects on the irradiance distribution of images. The recommendation on illumination pattern should hence be adjusted accordingly by calibrating the real imaging system

## 5.    EXPERIMENT IMPLEMENTATION

To investigate the optimized illumination plane, eye images were taken using a specialized setup that provided control over the required LED parameters.   A diagram of the setup is presented in Figure 11.   The LEDs were mounted inside a shell by two pivot points that served to control both the LED pitch and height.   The shell was mounted along an optical rail to allow axial movement of the LEDs.   A camera was mounted on a separate base and positioned along the optical axis to capture eye images.   The LEDs were positioned individually and the output irradiance pattern at the eye plane was matched to the simulated pattern by fine adjustment of the LEDs to compensate for deviation from nominal LED radiant intensity.   A chin rest was used to stabilize the head to situate the eye at the incident plane location.
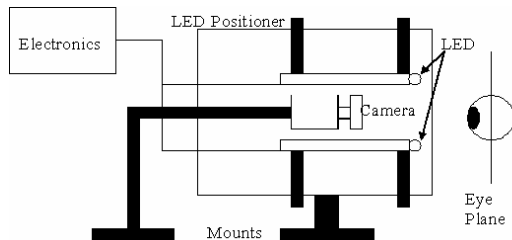


Figure 11:   Test system setup schematic

Eye images have been captured using illumination schemes created from the suggested LED parameters for $\delta = 0.3$ and $\delta = 0$ distributions.   A basic statistical method of analyzing skin area brightness mean and standard deviation has been used to score the



(a)



(b)

Figure 10:   LightTools® output of: (a) the optimized eye plane, and (b) the optimized image plane.

eye images.   The preliminary results indicate that the image for $\delta$ equal 0.3 scores better than images for $\delta$ equal 0, although many more incident plane patterns still need to be tested. Figure 12 shows the eye image for $\delta$ equal 0.3 and corresponding segmentation of the pupil and glints to highlight the identifiable features that are to be fed to eye tracking algorithms.

## 6.  CONCLUSIONS

In this paper, the foundation has been laid for using non-sequential ray trace software to optimize an illumination scheme for an integrated ET-HMD.   The effect of the illumination scheme is to allow for a better eye tracking capability due to the increase in efficiency of the eye tracking algorithms.   The optimization process involved creating a simulated model of a complete eye tracking system with adjustable LED parameters to control the illumination pattern on the eye plane.   Based on the simulations discussed in this paper, it is determined that a normal distribution with a falloff of $\delta$ equal 0.4±0.2 at the diagonal corners is expected to produce a "better" illumination for the pupil-based eye tracking system, compared to other values of $\delta$.

Ongoing research is concentrating on improving the optimization by utilizing parameters such as eye rotation and improving the eye feature reflectance model to be more robust. Gaussian illumination patterns with smaller $\delta$ increments, non-Gaussian illumination patterns, and methods of determining actual eye image quality for verification of simulation results are being investigated for a final implementation of an optimized illumination scheme into an integrated ET-HMD.
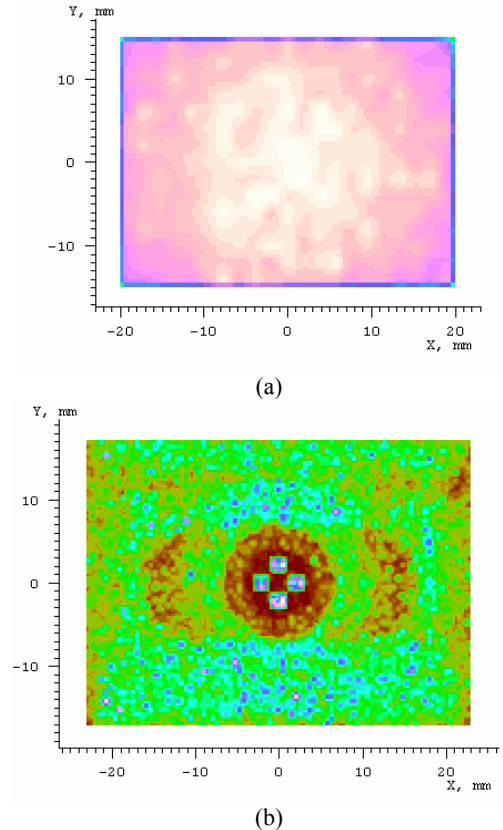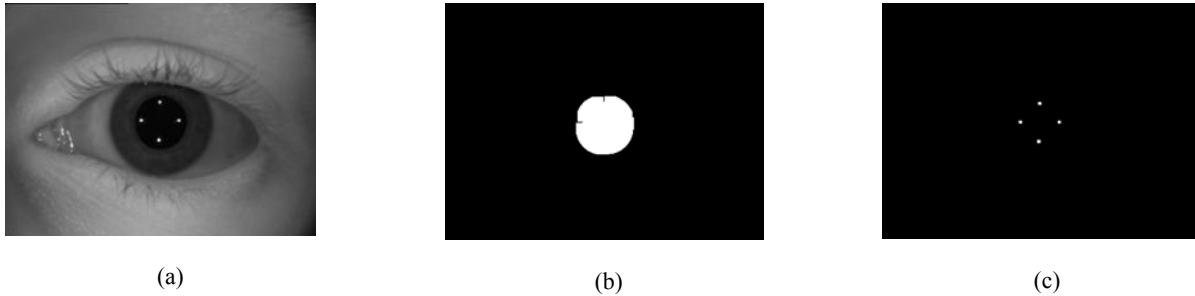
|  (a) | (b) | (c) |

Figure 12: (a) Eye image taken with δ = 0.7 incident plane, (b) pupil segmentation, and (c) glint segmentation

## ACKNOWLEDGEMENTS

## REFERENCES

1.  Ivan Sutheland, "The ultimate display," *Proceedings of IFIP 65*, **Vol. 2**, pp. 506-508, 1965.
2.  D. Buxton, G.W. Fitzmaurice, "HMDs, caves and chameleon: a human-centric analysis of interaction in virtual space," *Computer Graphics (ACM),* **Vol. 32(4)**, pp. 69-74, Nov. 1998.
3.  J.P. Rolland, D. Ariely, W. Gibson, "Towards quantifying depth and size perception in virtual environments," *Presense: Teleoperators and Virtual Environments (MIT Press),* **4(1)**, pp. 24-49, 1995.
4.  A. State, G. Hirota, D.T. Chen, W.E. Garrett, and M. Livingston, "Superior augmented-reality registration by integrating landmark tracking an magnetic tracking," *Proc. Of SIGGRAPH 1996, ACM SIGGRAPH*, pp. 429-438, 1996.
5.  H.L. Pryor, T.A. Furness, E. Viirre, "The Virtual Retinal Display: A New Display Technology Using Scanned Laser Light," *Proceedings of Human Factors and Ergonomics Society, 42$^{nd}$ Annual Meeting*, pp. 1570-1574, 1998.
6.  R. Fisher, *Head-mounted projection display system featuring beam splitter and method of making same*, US Patent 5,572,229, 1996.
7.  H. Hua , A. Girardot, C. Gao, and J.P. Rolland, "Engineering of head-mounted projective displays," *Applied Optics*, **39 (22)**: 3814-3824, August 2000.
8.  J.P. Rolland, and H. Fuchs, "Optical versus video see-through head-mounted displays in medical visualization," *Presence: Teleoperators and Virtual Environments*, **Vol 9(3)**, pp. 287-309, MIT Press, 2000.
9.  L.R. Young, D. Sheena, "Methods and Designs:   Survey of eye movement recording methods", *Behavior Research Methods and Instrumentation*, **Vol 7(5),** pp. 397-429, 1975.
10. G.H. Byford, "Non-linear relations between the corneo-retinal potential and horizontal eye movements," *Journal Physiol*. London, 168: pp. 14-15, 1963.
11. A.E. Kaufman, A. Bandopadhay, B.D. Shaviv, "An eye tracking computer user interface," *Proceedings IEEE 1993 Symposium on Research Frontiers in Virtual Reality*, IEEE Computer Soc. Press. 1993, pp. 120-1, Los Alamitos, CA USA.
12. D.A. Robinson, "A method of measuring eye movements using scleral search coil in a magnetic field," *IEEE Trans. Biomed. Electron.* BME **Vol. 10**, 137-145, 1963.
13. L. Ferman, H. Collewjin, T.C. Jansen, A.V. Van den Berg, "Human gaze stability in the horizontal, vertical and torsional direction during voluntary head movements, evaluated with a three-dimensional scleral induction coil technique," *Vision Research*, 27, pp. 811-828, 1963.
14. H. Hua, "Integration of eye tracking capability into optical see-through head mounted displays", *Proceedings of SPIE **Vol. 4297***, pp. 496-503, 2001.
15. C.W. Hess, R. Muri, O. Meienberg, "Recording of horizontal saccadic eye movements: Methodological comparison between electro-oculography and infrared reflection oculography," *Neuro-Opthamology*, 6: pp. 264-272, 1986.

16. A.T. Duchowski, "Incorporating the viewer's Point-Of-Regard (POR) in gaze-contingent virtual environments," *SPIE-Int. Soc. Opt. Eng. Proceedings of SPIE – The International Society for Optical Engineering*, **vol. 3295**, 1998, pp. 332-43.

17. G. Beach, C.J. Cohen, J. Braun, G. Moody, "Eye tracker system for use with head mounted displays," *Proceedings of the IEEE International Conference on Systems, Man and Cybernetics*, IEEE, Piscataway, NJ, USA, **Vol 5**, pp. 4348-4352, 1998.

18. L. Vaissie, J.P. Rolland, "Eyetracking in head-mounted displays: analysis and design", Technical Report TR98-007, University of Central Florida, 1998.

19. K. Iwamoto, S. Katsumata, K. Tanie, "An Eye Movement Type Head Mounted Display for Virtual Reality System: -Evaluation Experiments of a Proto-type System-", *IEEE*, pp. 13-18, 1994.

20. K. Iwamoto, K. Tanie, "High Resolution, Wide View Angle Head Mounted Display Using Eye Movement Tracking: -System Structure and Evaluation Experiments-," *IEEE*, pp. 289-294, 1995.

21. K. Iwamoto, K. Tanie, "An Eye Movement Type Head Mounted Display for Virtual Reality System: -Capturing and Displaying Real Environment Images with High Reality-", *IEEE*, pp. 3385-3390, 1997.

22. K. Iwamoto, K. Komoriya, K. Tanie, "Eye Movement Tracking Type Image Display System for Wide View Image Presentation with High-Resolution: -Evaluation of High-resolution Image Presentation-", *IEEE*, pp. 1190-1195, 2002.

23. J.P. Rolland, A.Yoshida, L.D. Davis, J.H. Reif, "High-resolution inset head-mounted display", *Applied Optics*, **Vol. 37(19)**, pp. 4183-4193, July 1998.

24. Optical Research Associates Website (2005):   http://www.opticalres.com.

25. A.W. Fitzgibbon, M. Pilu and R.B. Fisher, "Direct Least-Squares Fitting of Ellipses," *IEEE Trans. Pattern Analysis and Machine Intelligence,* **vol. 21**, no. 5, pp. 476-480, May 1999.

26. A. Atchison, G. Smith, *Optics of the Human Eye*, pp. 251-258, Butterworth-Heinemann, Woburn, MA, 2000.

27. J. Schwiegerling, Field Guide to Visual and Opthalmic Optics, pp. 16, SPIE Press, Bellingham, WA, 2004.

28. A. Atchison, G. Smith, *Optics of the Human Eye*, pp. 106, Butterworth-Heinemann, Woburn, MA, 2000.

29. S.R. Marschner, S.W. Westin, E.P.F. Lafortune, Kenneth E. Torrance, D.P. Greenberg, "Image-Based BRDF Measurement Including Human Skin", *10th Eurographics Workshop on Rendering*, pp. 139-152, Granada, Spain, June 1999.

30. J.G. Baker, *Highly corrected objective having two inner divergent meniscus components between collective components*, U.S. Patent 2,532,751, 1949.